Dilemma resolved: Airbrakes tamed

Michael Greiner and Galih Bangga
greiner@iag.uni-stuttgart.de
Institute of Aerodynamics and Gas Dynamics
University of Stuttgart, Stuttgart, Germany

Abstract

With increasing span or wing loading, it becomes increasingly difficult to fulfill all CS22 certification requirements for airbrakes simultaneously. Aerodynamic forces upon Schempp-Hirth airbrakes usually create pilot control forces, which limit the size of the airbrake. A certain design of the airbrake allows to reduce the aerodynamic source of this force considerably. This also solves two safety issues: It allows the pilot to retract the airbrakes at high speed and also reduces the risk of self extension of unlocked airbrakes at take-off.

Introduction

Airbrakes for sailplanes have been a topic for research since the 1930ies [1]. Since early 1980ies all new serial production sailplanes use Schempp-Hirth-type airbrakes extending on the upper side of the wing. This document refers only to this variant. Alternative solutions are discussed only rarely [2].

This kind of airbrakes is efficient in controlling the glide path, because they not only create pressure drag, but also induced drag. This is because they locally reduce lift as if the angle of attack would be reduced by about 12° as can be seen in measurements by Althaus [3]. Handling is usually considered good-natured, since the ensuing decrease of wing lift coefficient is compensated by an increase of trim speed. Available literature on the topic of these airbrakes concentrate on the effect upon lift, drag and aerodynamic moment of different 2D- and 3D-configurations [3–10].

Figure 1 shows a typical Schempp-Hirth airbrake with its main components. Realizations with a single panel only are unusual nowadays on new designs: because of little space due to thinner airfoils and shorter chords, and because of high wing loadings and greater spans, which require larger frontal area. A common configuration is the one depicted in Fig. 1 and Fig. 2, with the upper panel located in front of the levers, and one or two lower panels located behind. It has the advantage that the rear edge of the cut-out in the wing skin supports the lower panel(s).

Presented at the XXXIV OSTIV Congress, 28 July – 3 August 2018, Hosin, Czech Republic

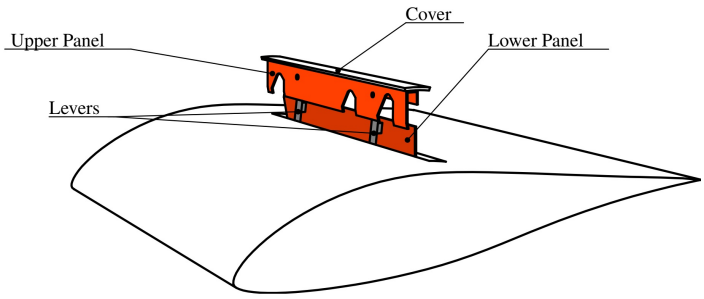

Fig. 1: Components of a Schempp-Hirth airbrake.

Despite all their advantages, for the designer of modern sailplanes, Schempp-Hirth-type airbrakes have constituted a problem in a different respect. As soon as the airbrakes are unlocked, a vertical aerodynamic force pulls the airbrakes up. At approach speeds this force may be small, and countered by weight and friction. But this aerodynamic force increases heavily with airspeed. Relevant for the pilot control force is only the component F_y parallel to the direction of extension. The index y refers to the local 2D coordinate system that may be slanted together with the airbrake.

All common airworthiness codes from obsolete LFSM [11] to CS22 [12] require not only a glide slope not flatter than 1:7 during approach, and certain speed limiting capabilities at high speed. They also require that the pilot control force F_p for retracting the airbrake does not exceed 20daN at certain speeds (Table 1). With increasing wing loadings and glide ratios, this becomes increasingly difficult to fulfill simultaneously. The involved requirements have continuously been softened since the introduction of LFSM in 1975, which proves the ongoing existence of this dilemma. It adds to the problem that none of the required properties can be predicted in advance with simple methods and necessary precision.

The vertical aerodynamic force upon the airbrake is also responsible for the vicious characteristic that unlocked airbrakes extend themselves during launch, preventing the normal climb to safe altitude. This has been the reason for various accidents during winch-launch, aerotow as well as self-launch. In fact the

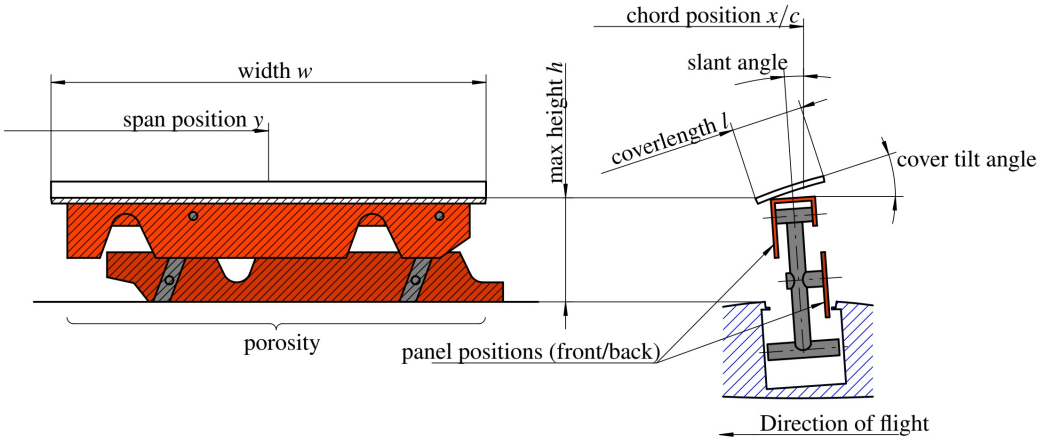

Fig. 2: Parameters in the design of an airbrake; porosity describes how tight the airbrake is (compare hatched area with area $h \cdot w$ and consider gap between upper and lower panel).

LFSM (1975)	**CS22 (2003)**
LFSM 2125	**CS 22.75 Descent Approach**
Glide slope not flatter than 1:7 at $1.3V_{S0}$	
LFSM 2601 With airbrake extended, sailplane will not exceed V_{NE} in a dive of 45°	**CS 22.73 Descent, High Speed** With airbrake extended, sailplane will not exceed V_{NE} either in a dive of 30° or at sink rate of more than 30m/s. [For aerobatic or cloud flying a dive of 45° is still required.]
LFSM 2611 & 2155 Must be possible to retract airbrakes up to $0.75V_{NE}$ with a hand force not exceeding 20daN	**CS 22.697(c)(2) Wing flaps and airbrake controls** Must be possibe to retract airbrakes up to V_T [min 125km/h], but not less than $1.8V_{S1}$, with a hand force not exceeding 20daN
LFSM 4243	**CS 22.697(b) Wing flaps and airbrake controls**
Each wing-flap and airbrake must be designed to prevent inadvertent extension or movement. [..]	

Table 1: Comparison of requirements concerning airbrakes in LFSM [11] and CS22 [12]: efficiency, pilot control forces and inadvertent extension.

airworthiness codes at all times have required that inadvertent extension must be prevented by design (see again Table 1). It seems that authorities and sailplane manufactures considered a lock, which keeps the airbrake in the fully retracted position, as sufficient. Only a few years ago, additionally the so called Pigget-Hook was introduced in few sailplane types. This hook catches the airbrake lever of an unlocked airbrake. Other means of improving the situation are additional springs, friction elements, or coupled flaps. Such measures make the design more complicate and expensive.

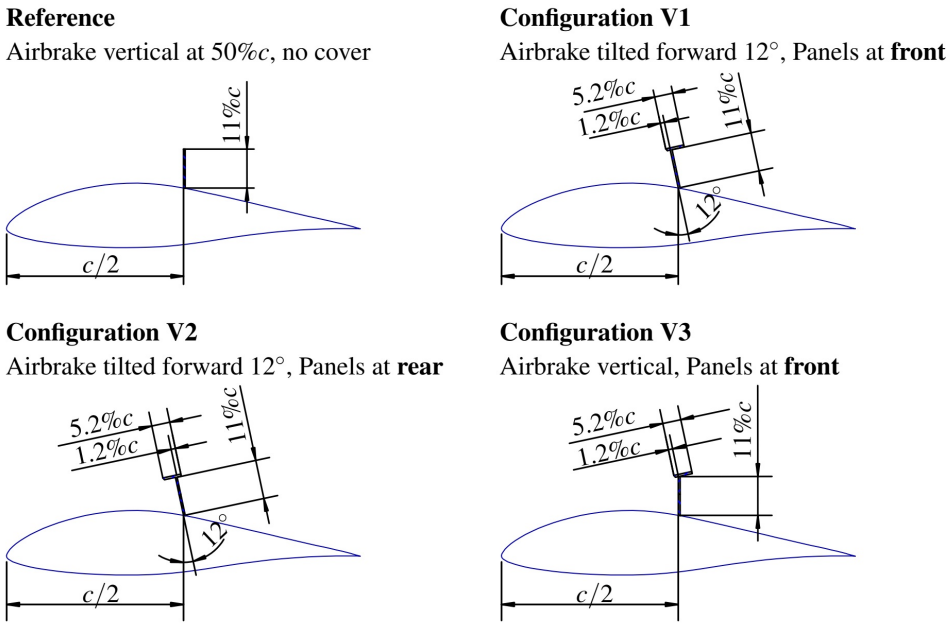

Fig. 3: Configurations examined in CFD (Airfoil FX 66-17AII-182, $Re = 1.5 \cdot 10^6$; the reference case is comparable to measurements performed in [3] for $c_l(\alpha)$; Configurations V1 to V3 are calculated for $\alpha = 0°$).

Another troublesome feature is connected with high airspeeds. The airworthiness codes require the airbrake also to be a means to limit the airspeed in a steep dive. But the aerodynamic force makes it impossible to retract in this speed range. Once opened, the airbrake will stay fully extended throughout the recovery from the dive - because in most sailplanes, the pilot is not capable of retracting the airbrakes unless at lower airspeed. This is unfavorable, because extended Schempp-Hirth airbrakes not only increase the loss of altitude during the pull-out, they also increase the wing bending moment. Only a limit load factor of 3.5g is required with airbrakes extended at high speed, and this load case is often the most critical for the wing.

The goal of the present investigation is to strike at the root of the problem, and to reduce the aerodynamic force F_y, which acts in direction of airbrake extension. With some general considerations and specific CFD-calculations, it shall be clarified what is useful and necessary to diminish F_y.

State of Development

Approaches to reduce F_y were described in Schaum [13], where it was proposed to tilt the cover by 30° and introduce a gap between cover and upper panel, to reduce the static pressure below the cover. This is mainly a structural thesis with no aerodynamic validation. Greiner [14] reported for a new sailplane design with an airbrake comparable to configuration V1 of Fig. 3 that the control force of the airbrakes is neutral at all speeds flown, and that the airbrakes would remain at their position during approach even when released. It was assumed that this is due to the slant forward airbrakes.

Among existing sailplanes there is already a wide range of configurations, see Table 2. Some already exhibit single features, which will be recommended in the conclusion of this article. But there is no distinct trend discernible. In general, experiences with different sailplane types are difficult to compare, since it can be expected that the control systems differ in their extreme values of gearing ratios. This makes this investigation necessary.

Methodology

The variables in the design of the airbrake are identified in Fig. 2. Due to the size of force F_y we can assume that it results from pressure differences, not from wall shear. The cover area lw is the only suitable surface for a pressure difference to act upon, because the panels are parallel with the direction of extension. Therefore F_y is proportional to lw, and lwh is proportional to the work required to retract the airbrake. This work is equal to the work applied by the pilot $F_p \cdot s$, where F_p is the pilot control force, and s is the travel of the cockpit control, while friction is neglected. When s and l are considered constant due to other constraints, then the pilot control force F_p is proportional to the product of airbrake width w and maximum height h of the extended airbrake.

$$F_p \propto w \cdot h$$

This leads to two tasks:

1. For a required drag increase effect, make the airbrake as efficient as possible, to allow a small as possible wh.
2. For a given wh, design the airbrake in a way to reduce the aerodynamic force in direction of extension F_y.

Type	Year of first flight	Number of Panels	All panel(s) in front of levers	All panel(s) behind levers	Upmost panel before levers Lowest panel behind	Cover tilted	Airbrake slanted forward
Astir CS	1974	1		X			
Twin Astir	1976	1		X			
LS 3	1976	2			X		
ASW 20	1977	1	X				
ASK 21	1979	1	X				
Ventus	1980	2	X				
ASW 22, ASH 25	1981	2			X		
DG 300	1983	1	X				
Discus	1984	2	X				
ASW 24	1987	2			X		
DG 500	1989	2			X		
ASH 26	1993	2			X		
DuoDiscus	1993	2	X				
LS 8	1994	2			X		
Ventus 2	1994	2	X				
ASW 27, ASG 29	1995	3			X	X	
Discus 2	1998	2	X				
ASW 28	2000	2			X	X	
Arcus	2009	3			X		
ASG 32	2014	2	X			X	X
Ventus 3	2016	3		X			X
Recommendation			X			X	X

Table 2: Airbrake configurations of various sailplane types, sorted by year of first flight.

Task 1: More Drag per Frontal Area

A number of parameters from Fig. 2 has to be considered, when optimizing the drag of the airbrake. This task can be based on available data from literature. The chord position x/c does not seem to be too important, as long as it stays within usual limits [4, 9].

Figure 4 shows the drag coefficient C_{Do} of rectangular plates (upper curve) as a function of their height to span ratio (h/b), [7]. Below an aspect ratio of $(h/b) = 0.2$ the drag coefficient increases with decreasing aspect ratio. The aspect ratio of the airbrake may have to be calculated as $(h/b) = 2h/w$ for this diagram, since the wing surface represents a mirror boundary condition. With typical values such as $h = 150$mm and $w \leq 1400$mm, the airbrake is just not yet in the range where the aspect ratio matters. Still width is more effective than height to reduce wing lift. On the other hand the designer is interested in restricting the width of the airbrake, because of the distortion

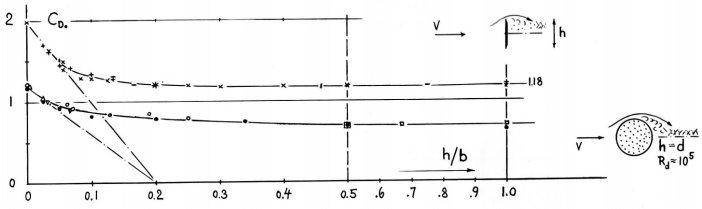

Fig. 4: From Hoerner [7], Fig. 28, chapter III: *Drag coefficients of rectangular plates and circular cylinders as a function of their height (or diameter) to span ratio*.

in the wing surface around the cover in the retracted state.

Airbrakes of powered airplanes often comprise slits and holes to reduce buffeting. For sailplanes this is not necessary, because the airbrake can be located between aileron and horizontal tail. Hoerner [7] states that *the drag coefficient (on flap area) of and due to a pervious flap is somewhat smaller than that of the solid type*, see Fig. 5. In some literature, care has to be taken when using data concerning configurations with and without a gap between panel and airfoil surface. Usually authors assume that the panel height is limited because of the given wing thickness, and therefore create the gap by moving the same panel upwards. In this case the gap increases drag, but the airbrake also reaches out further into the flow field. In this investigation one basic prerequisite is that the max height h from wing surface to the cover is limited due to pilot control forces. When the additional drag – measured in configurations with and without gap – is put in relation to the max height h, a configuration without gap produces equal or more drag per height. This applies to the data of Fig. 42 from Straub [10] and to the data of Table 1 from Pátek [9].

A low porosity requires that all airbrake panels are installed on the same side of the levers, either in front or at the rear, and that the axles of the levers are located very low. Figure 6 depicts the design from [14], showing that a design without many cutouts is possible.

Figure 7 shows that the drag of a fold with the open side

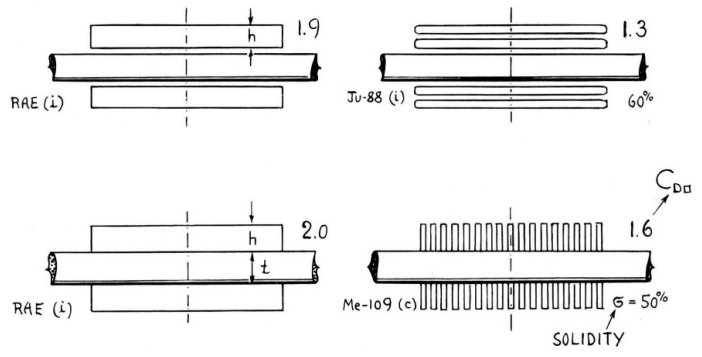

Fig. 5: From Hoerner [7], Fig. 30a, chapter III: *Drag of and due to dive brakes [...]; all part-span; t/c between 12 and 14%; x/c between 30 and 40%*.

Fig. 6: Example for a tight airbrake (ASG 32): Both panels on the same side and only little cut-outs (Photo: Adolf Wilsch).

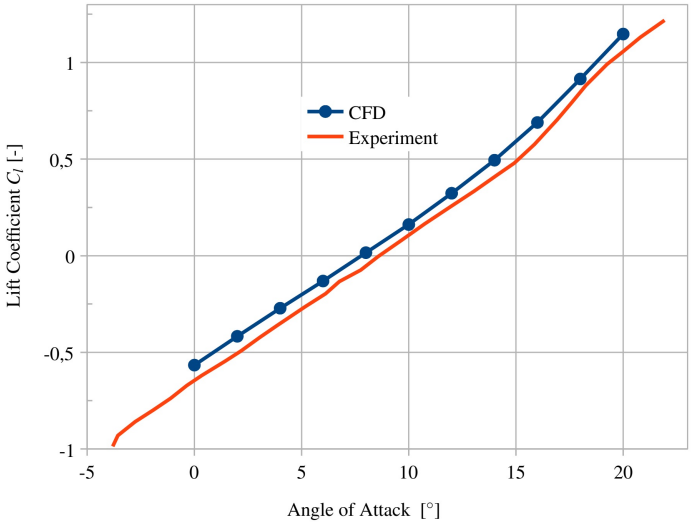

Fig. 8: Lift versus angle of attack, reference configuration; experimental data from Althaus [3].

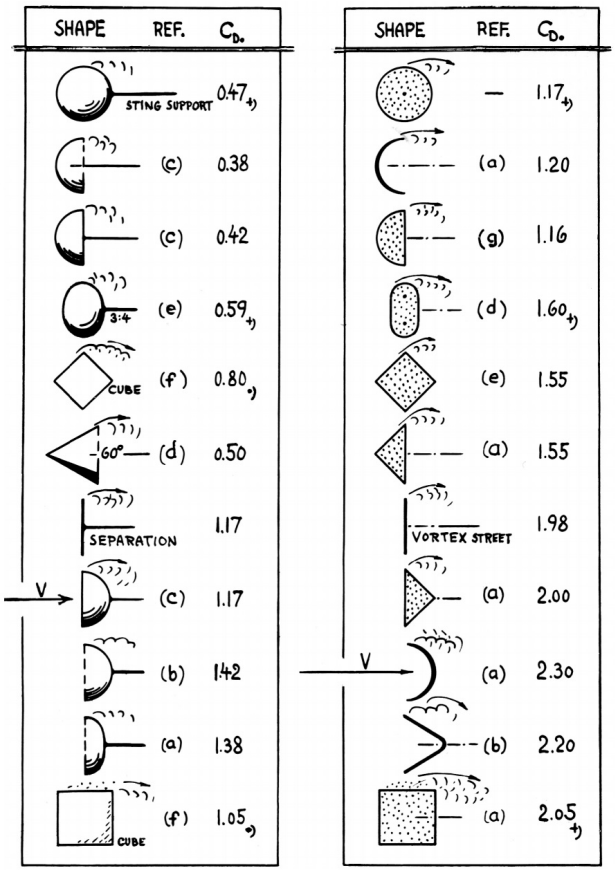

Fig. 7: From Hoerner [7], Fig. 33, chapter XIII: *Drag coefficients [...] of 2-dimensional shapes (between walls) at R between* 10^4 *and* 10^6 *[...].*

against the stream is larger than the drag of a flat plate [7]. An airbrake slant forward and mirrored in the wing surface can be seen as such a fold, and should therefore have a higher drag than a vertical airbrake.

Task 2: Less Pilot Control Force per Frontal Area

For the second task other parameters may be relevant. The cover length l can only be reduced to a limited degree, due to structural constraints and maintenance needs.

For the ASW 27 glider, Gerhard Waibel introduced a cover, which tilts a few degrees upon extension (cover tilt angle), but this measure is limited, due to the necessary kinematics. Two parameters remain, first the position of the panels, i.e. behind or in front of the levers, and second the slant angle of the whole airbrake.

To investigate both parameters, three 2D-configurations were defined (Fig. 3), which were investigated with the aid of CFD. In order to validate the CFD, a reference case was taken from [3], namely the airfoil FX 66-17AII-182 with a single vertical panel

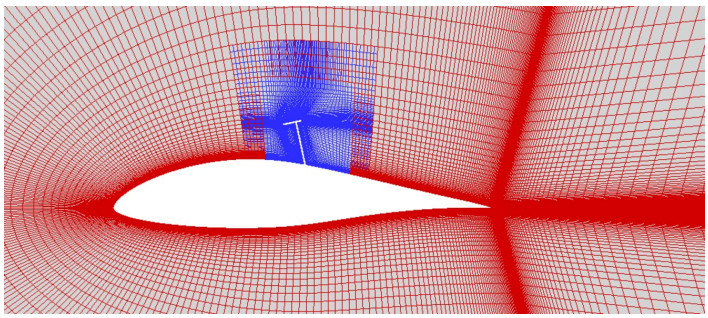

Fig. 9: Grid composed from two structured grids employing the Chimera method.

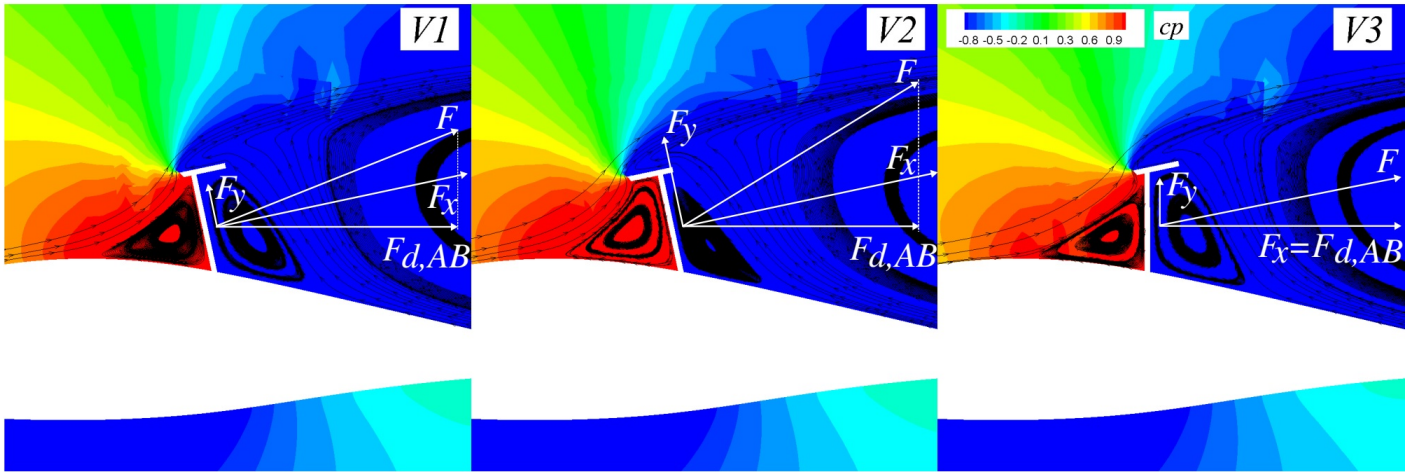

Fig. 10: Pressure distributions and streamlines at $Re = 1.5 \cdot 10^6$, $\alpha = 0°$, $h/c = 11\%$, $x/c = 50\%$.

at $x/c = 50\%$ and with a height of $h/c = 11\%$ ($Re = 1.5 \cdot 10^6$), see Fig. 8 for comparison of $c_l(\alpha)$. No drag measurements are available from [3]. The investigated configurations maintain the $h/c = 11\%$ and use a typical value of $l/h = 47\%$, to keep the local geometry similar to a typical extended airbrake.

The airbrakes of configurations V1 and V2 are slanted forward 12°. In V1, the panels are in the front, leaving only little forward protrusion of the cover. The second configuration V2 has the panels at the rear. The third configuration V3 differs from V1 in that the airbrake extends normal to the chord.

The configuration depicted in Fig. 1 and Fig. 2, with the upper panel located in front of the levers, and the lower panel(s) located behind, was not included. It has a large porosity (reduced drag) and due to the deflection of the airflow between the panels, it is not very promising with respect to pilot control force.

The 2D simulations were carried out using the CFD code FLOWer developed by the German Aerospace Center (DLR) [15]. The code has been extended in the recent years for aircraft and wind turbine simulations at IAG [16, 17]. The turbulence closure was modeled using the Shear-Stress-Transport (SST) k-model according to Menter [18]. The model was shown in previous studies to be able to model flow separation on airfoils and 3D rotors accurately for reasonable angle of attack operations [16, 18, 19]. The time dependent solution of the URANS model was integrated using the dual-time-stepping approach, allowing a second order accuracy on smooth meshes. The hybrid 5-stages Runge-Kutta scheme was employed for this purpose. The time step size was set to be less than 0.01 of the convective time required for a fluid particle to pass the airfoil. The spatial discretization uses a central discretization approach. Convergence was accelerated by means of the multigrid level 3 scheme. The grid was generated using the software Pointwise employing a Chimera (overset) method (Fig. 9). By doing so, high quality meshes can be built separately, simplifying the generation of the meshes significantly. The airfoil is resolved by 281 x 129 grid points on the airfoil surface and in normal direction, respectively. The boundary layer is discretized by 32 cells with the growth rate of 1.1 and a non-dimensional wall distance of $y^+ < 1$. The latter is required to resolve the boundary layer as no wall model is used. The simulations were performed on the High Performance Computing Center Stuttgart (HLRS) on the LAKI cluster employing 24 CPUs for each simulation.

Results

Figure 10 shows the pressure distribution and streamlines of the three configurations. Some features are plainly visible: In front of the panels as well as behind, there are large separations. The streamlines in front of the airbrake ascend under an angle of approximately 60° to the panels and overshoot considerably when crossing the leading edge of the cover. Figure 11 from [10] shows an experiment in the water tunnel for comparison. The Re-number is smaller, and the relative height of the airbrake is larger, nevertheless the features of the flow are well comparable. Due to the direction of the flow, the cover upper surface is sepa-

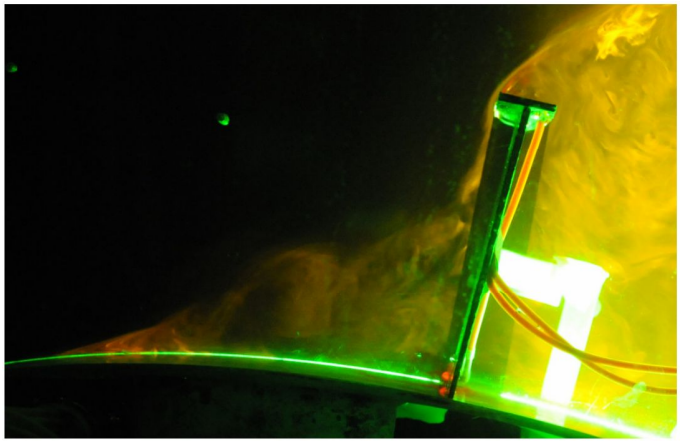

Fig. 11: Experiment, airfoil st3, $Re = 6.6 \cdot 10^4$, $\alpha = 5°$, $h/c = 27\%$, $x/c = 55\%$ (Fig. 37 from Straub [10]).

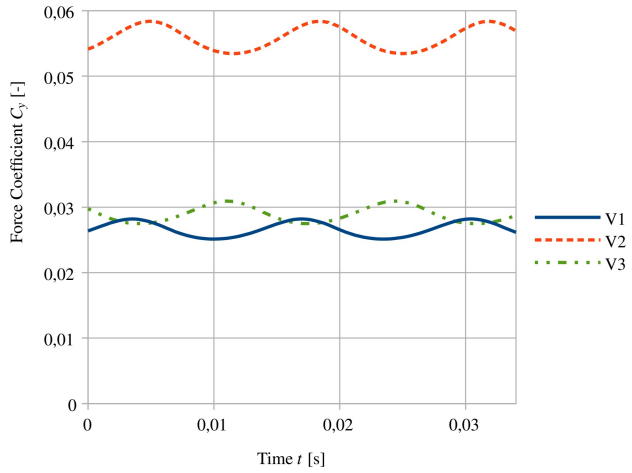

Fig. 12: Force coefficient C_y in direction of extension.

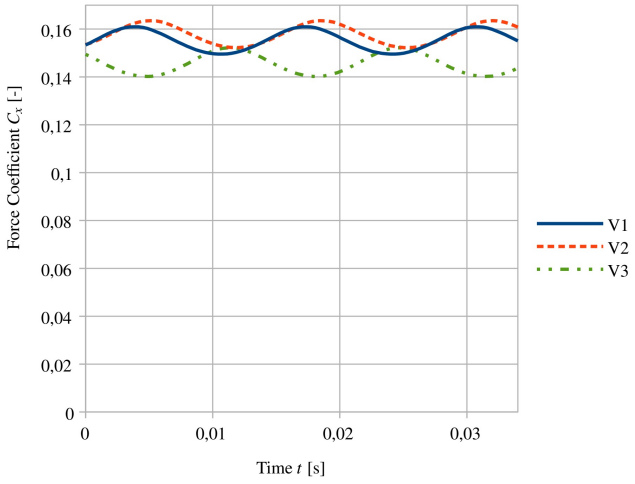

Fig. 13: Force coefficient C_x normal to panel.

rated. This might only be prevented by tilting the cover more than 40°, which would be difficult mechanically. Therefore, with the airbrake extended so far up, tilting the cover by few degrees presumably has little effect. Plots of the pressure distributions in Fig. 10 also show that almost the stagnation pressure acts on the whole front of the panel, and a pressure coefficient of about -0,8 acts on top and behind the airbrake, at least as long as the airbrake is tight and for the 2D-case.

The force upon only the airbrake components was calculated, separated in a component normal to the airbrake panel (F_x/dz) and in direction of extension (F_y/dz). The pressure and skin friction distributions were integrated for this purpose over the cover and the panel. Pressure forces are three orders of magnitude larger than friction forces. The calculated forces are normalized by the free stream conditions as:

$$C_{x,y} = F_{x,y}/(\frac{1}{2}\rho_\infty V_\infty^2 cdz)$$

Figure 12 and Fig. 13 show Cy and Cx over time. The fluctuations result from the shedding of vortices, see Fig. 14. The average values are given in Table 3, and are drawn into Fig. 10. The values are plausible, but cannot be used directly for design purposes, because the relative cover length l/c is smaller than typical values, and on real wings additional 3D effects occur.

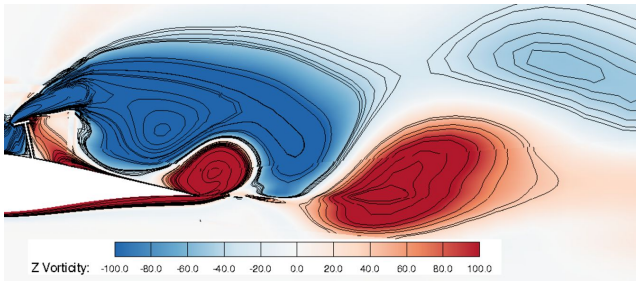

Fig. 14: Vorticity in the flow field resulting in oscillations of the force coefficients.

The position of the airbrake panels in front or behind the levers has a strong influence on the extension force F_y. With the panels installed in the front, the force F_y is reduced by half compared to case V2. With the panels mounted on the front side, slanting the airbrake forward has a favorable influence on F_y and F_x, but a considerably smaller one. When discussing the amount of drag created by the airbrake itself, the component of $(F_x + F_y)$ in direction of the flow, $F_{d,AB}$, should be considered (see Table 3, with the drag force $F_{d,AB}$ expressed by its normalized coefficient $C_{d,AB}$). Configurations V1 and V3 actually have the same $C_{d,AB}$, but the relation between additional drag and aerodynamic pilot control force $(C_{d,AB}/C_y)$ is best for configuration V1.

This result is in accordance with the experience reported in [14], except that slanting the airbrake seems not to be the major contribution. It should be remarked that another parameter has not been investigated, namely the angle of attack. It might be possible that the influence of slanting differs at high speed (i.e. at less angle of attack). The result for panels at the front is also in accordance with the authors experience with the ASW20 (see Table 2), which has manageable airbrake control forces even at 180km/h. But as mentioned above, experience with different sailplane types cannot be compared easily, due to the influence of the different control kinematics.

Configuration	C_y [-]	C_x [-]	$C_{d,AB}$ [-]	$C_{d,AB}/C_y$ [-]
V1	0.0265	0.1552	0.1463	5.5
V2	0.0559	0.1578	0.1427	2.6
V3	0.0292	0.1463	0.1463	5.0

Table 3: Mean force coefficients for the three configurations; $C_{d,AB}/C_y$ is a measure for the relation between pressure drag and pilot control force.

Conclusions

In first approximation, the pilot control force F_p is proportional to the product of airbrake width w and maximum height h

of extension. To achieve the required drag increase with a small as possible frontal area $w \cdot h$, and to achieve a small as possible pilot control force F_p for this frontal area, design the airbrake according to the following recommendations:

- The panels should be mounted in front of the levers.
- The cover should protrude before the panels as little as possible.
- The panels should be tight, ...
    1. to maintain a high pressure difference at the panels.
    2. to maintain a low pressure under the cover behind the panels.
- In this configuration: Slanting forward the airbrake is favorable.
- The cover angle was not studied in this investigation, but a slight tilt seems favorable in various sailplane types, presumably in cases when the airbrake is extended only a little.
- Besides the aerodynamics, the control kinematics must not develop unfavorable gearing ratios in any position. But this is a topic outside the scope of this investigation.

Acknowledgements

The authors would like to thank Prof. Ewald Krämer for the opportunity to conduct this work at the Institute of Aerodynamics and Gasdynamics and Dr. Ing. Werner Würz for his support.

References

[1] Jacobs, H. and Wanner, A., "DFS Sturzflugbremsen an Segel-und Motorflugzeugen." *Jahrbuch 1938 der deutschen Luftfahrtforschung, Luftwissen*, Vol. 4, No. 7, 1937, pp. I 313 – I 318, translated and republished as NACA-TM-926.

[2] Gedeon, J., "A few words on airbrakes." *Technical Soaring*, Vol. 31, No. 4, 2007, pp. 110 – 113.

[3] Althaus, D. and Wortmann, F. X., *Stuttgarter Profilkatalog I*, Friedrich Vieweg & Sohn, Braunschweig, Germany, 1981, pp. 260 – 286.

[4] Arnold, K. O., "Aerodynamische Untersuchungen an Flügeln mit Bremsklappen." *ZFW Zeitschrift für Flugwissenschaften und Weltraumforschung*, Vol. 14, No. 6, 1966, pp. 276 – 281.

[5] Flower, J., "Lift and rolling moment due to spoilers on wings with flaps undeflected at subsonic speeds." Esdu 90030, Royal Aeronautical Society, London, 1999.

[6] Green, M. J., "Drag and yawing moment due to spoilers." Esdu 96026, Royal Aeronautical Society, London, 1999.

[7] Hoerner, S. F., *Fluid Dynamic Drag*, Hoerner Fluid Dynamics, Bakersfield, CA, USA, 1965, pp. 3-14 – 3-17 and pp. 13-11 – 13-12.

[8] Merklein, H. J., "Bestimmung aerodynamischer Beiwerte durch Flugmessungen an 12 Segelflugzeugen mit Brems- und Landeklappen." FFM-Bericht 63, Flugwissenschaftliche Forschungsanstalt e.V., München, 1963.

[9] Pátek, Z., Cervinka, J., and Vrchota, P., "Wind tunnel and CFD study of airfoil with airbrake." 28th International Congress of the Aeronautical Sciences, 2012.

[10] Straub, J., *Experimentelle Untersuchungen zur Wirksamkeit von Störklappen bei Segelflugzeugen*, Student research project, Institute of Aerodynamics and Gas Dynamics, University Stuttgart, 2009.

[11] LFSM, "Lufttüchtigkeitsforderungen für Segelflugzeuge und Motorsegler." Anlage zur 1. DV LuftBauO-LFSM, Bundesanzeiger Nr. 204 vom 31. Oktober 1975, 1975.

[12] EASA, "Certification Specifications for Sailplanes and powered Sailplanes CS22." European Aviation Safety Agency, Cologne, Germany, 2004.

[13] Schaum, A., *Konstruktion von Bremsklappen für Segelflugzeuge und Motorsegler mit dem Ziel der Erreichbarkeit niedriger Bedienkräfte*, Diploma thesis, Technische Hochschule Mittelhessen, Fachbereich Maschinenbau, 2011.

[14] Greiner, M., "Schleichers 20m Doppelsitzer: Was die ASG 32 ausmacht." Presentation at the symposium for sailplane development, Braunschweig, 2014.

[15] Kroll, N., Rossow, C. C., Becker, K., and Thiele, F., "The MEGAFLOW project." *Aerospace Science and Technology*, Vol. 4, No. 4, 2000, pp. 223 – 237.

[16] Bangga, G., Weihing, P., Lutz, T., and Krämer, E., "Effect of computational grid on accurate prediction of a wind turbine rotor using delayed detached-eddy simulations." *Journal of Mechanical Science and Technology*, Vol. 31, No. 5, 2017, pp. 2359 – 2364.

[17] Weihing, P., Letzgus, J., Bangga, G., Lutz, T., and Krämer, E., "Hybrid RANS/LES Capabilities of the Flow Solver FLOWerApplication to Flow Around Wind Turbines." *Symposium on Hybrid RANS-LES Methods*, Springer, Cham, 2016, pp. 369 – 380.

[18] Bangga, G., Hutomo, G., Wiranegara, R., and Sasongko, H., "Two-equation eddy-viscosity turbulence models for engineering applications." *AIAA journal*, Vol. 32, No. 8, 1994, pp. 1598 – 1605.

[19] Bangga, G., Hutomo, G., Wiranegara, R., and Sasongko, H., "Numerical study on a single bladed vertical axis wind turbine under dynamic stall." *Journal of Mechanical Science and Technology*, Vol. 31, No. 1, 2017, pp. 261 – 267.